10

Gas-Solid Flow Applications for Powder Handling in Industrial Furnaces Operations

Paulo Douglas Santos de Vasconcelos[1]
and André Luiz Amarante Mesquita[2]
[1]*Albras Alumínio Brasileiro S/A*
[2]*Federal University of Pará*
Brazil

1. Introduction

Gas-solid flow occurs in many industrial furnaces operations. The majority of chemical engineering units operations, such as drying, separation, adsorption, pneumatic conveying, fluidization and filtration involve gas-solid flow.

Poor powder handling in an industrial furnace operation may result in a bad furnace performance, causing errors in the mass balance, erosion caused by particles impacts in the pipelines, attrition and elutriation of fines overloading the bag houses. The lack of a good gas-solid flow rate measurement can cause economic and environmental problem due to airborne.

The chapter is focused on the applications of powder handling related with furnaces of the aluminum smelters processes such as anode baking furnace and electrolytic furnace (cell) to produce primary aluminum.

The anode baking furnace illustrated in figure 1 is composed by sections made up of six cells separated by partitions flue walls through which the furnace is fired to bake the anodes. The cell is about four meters deep and accommodates four layers of three anode blocks, around which petroleum coke is packed to avoid air oxidation and facilitate the heat transfer. During the baking process, the gases released are exhausted to the fume treatment center

(a) (b)

Fig. 1. a) Anode baking furnace building overview; b) Petroleum coke being unpacked from anode coverage by vacuum suction.

(FTC) where the gases are adsorbed in a dilute pneumatic conveyor and in an alumina fluidized bed. The handling of alumina is made via a dense phase conveyor.
The baked anode is the positive pole of the electrolytic furnace (cell) which uses 18 of them by cell. The pot room and the overhead multipurpose crane are illustrated in figure 2.

(a) (b)

Fig. 2. a) Aluminum smelter pot room, b) Overhead crane being fed of alumina from a day bin by a standard air slide.

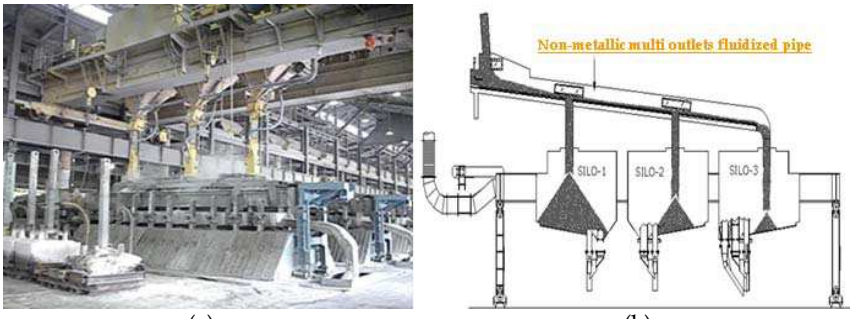

(a) (b)

Fig. 3. a) Electrolytic furnace being fed of alumina by the overhead crane; b) Sketch of electrolytic furnace being continuous fed of alumina by a special fluidized pipeline.

The old aluminum smelters feed their electrolytic cells with the overhead cranes as can be seen in figures 2 and 3. This task is very hard to the operators and causes spillage of alumina to the pot room workplace. This nuisance problem is being solved by the development of a special multi-outlets nonmetallic fluidized pipeline.
The fundamentals of powder pneumatic conveying and fluidization will be discussed in this chapter, such as the definition of a pneumatic conveying in dilute and dense phase, the fluidized bed regime map as illustrated in figure 5 and finally the air fluidized conveyor.
Firstly, petro coke and alumina used as raw materials in the primary aluminum process is characterized using sieve analyses (granulometry size distribution). Then, bulk and real density are determined in the laboratory analyses; with these powder physical properties, they can be classified in four types using the Geldart's diagram as illustrated in figure 4.

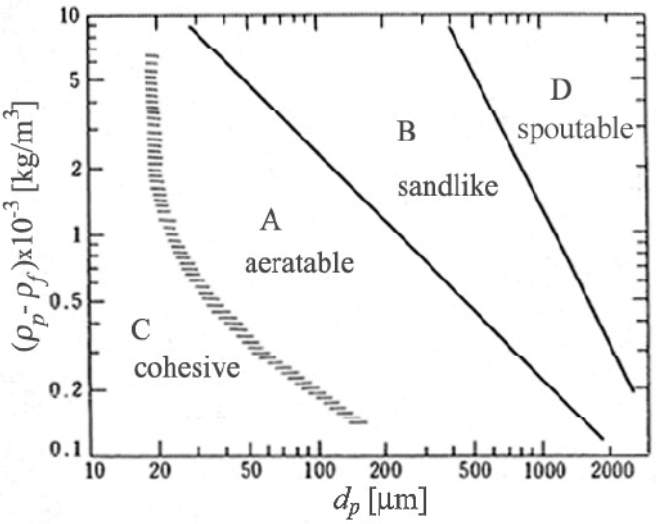

Fig. 4. Powder classification diagram for fluidization by air – source: (Geldart, 1972).

The majority of powders used in the aluminum smelters belong to groups A and B considering Geldart's criteria.

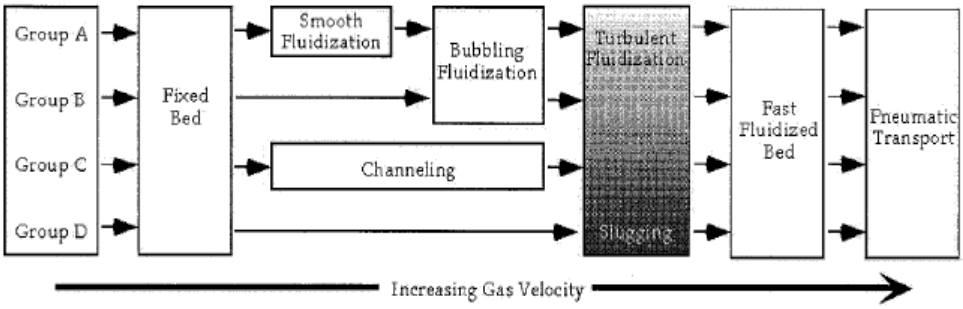

Fig. 5. Flow regime map for various powders.

This figure 5 summarized the fluidized bed hydrodynamics related with powders classified according to Geldart's criteria.

Once the velocities associated with each mode of operation are determined, the pressure drop of the regime is calculated so that the gas-solid flow is predicted using the modeling and software adequated to optimize the industrial installation.

The pipeline and air fluidized conveyors feeding devices are also discussed in this chapter.

Finally two cases studies applied in the baking furnace of pneumatic powder conveying in dilute phase are shown as a result of a master degree dissertation. Another case study is the development of an equation to predict the mass solid flow rate of the air-fluidized conveyor as a result of thesis of doctorate. The equation has design proposal and it was used in the design of a fluidized bed to treat the gases from the bake furnace and to continuously alumina pot feeding the electrolyte furnaces to produce primary aluminum.

2. Fundamentals of pneumatic conveying of solids

Pneumatic conveying of solids is an engineering unit operation that involves the movement of millions of particles suspend by draft in dilute phase or in a block of bulk solids in dense phase inside a pipeline. Figure 6 illustrates a pneumatic conveying of solids with the essential components, like the air mover, feeding device, pipeline and bag house.

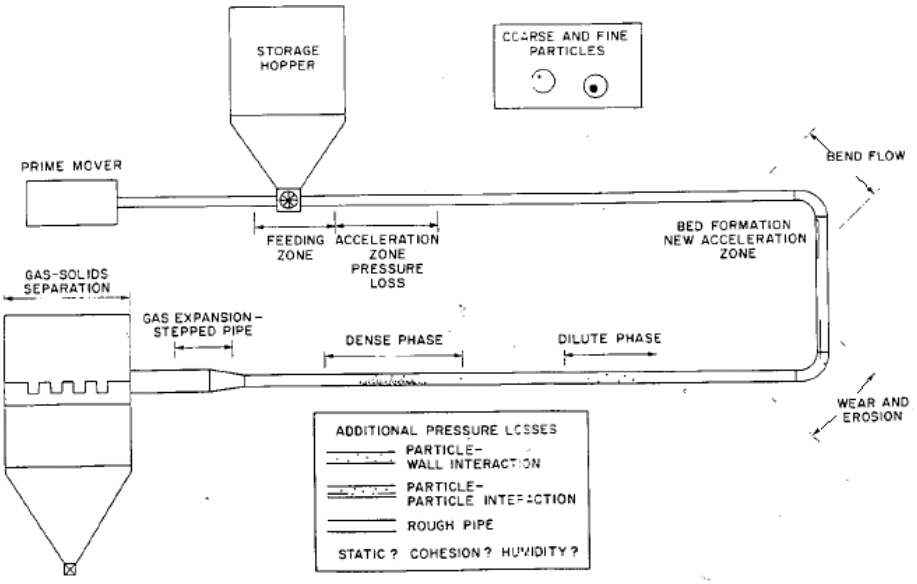

Fig. 6. Typical pneumatic conveyor layout – source: (Klinzing *et al*, 1997).

A good criterion showed in table 1 to decide if the transport of solids in air will be in dilute phase or in dense phase is the mass load ratio (μ) calculated by the equation 1.

$$\mu = \dot{G} \Big/ \dot{v}\,\rho_g \tag{1}$$

Where $\dot{G}$, $\dot{v}$ and ρ_g are the solid mass flow rate, gas (air) volume flow rate and gas (air) density.

Mode of transport of solids	Solids –to – air ratio (μ)
Dilute phase	0 - 15
Dense phase	> 15

Table 1. Systems' classification concerning solids-to-air ratio - source: (Klinzing et al, 1997).

Figure 7 illustrates a variety of solids modes of transportation and the states diagrams showing the log of the pipeline pressure drop versus the log of the air velocity inside the pipeline. From figure 7 it is concluded that in dilute phase the pneumatic conveyor has high air velocity, low mass load ratio, and low pressure drop in the pipeline. In dense phase mode the conveyor operates with high mass load rate, low air velocity but high pressure

drop in the pipeline. The engineer responsible for the project has to analyze which is the best solution for each case study.

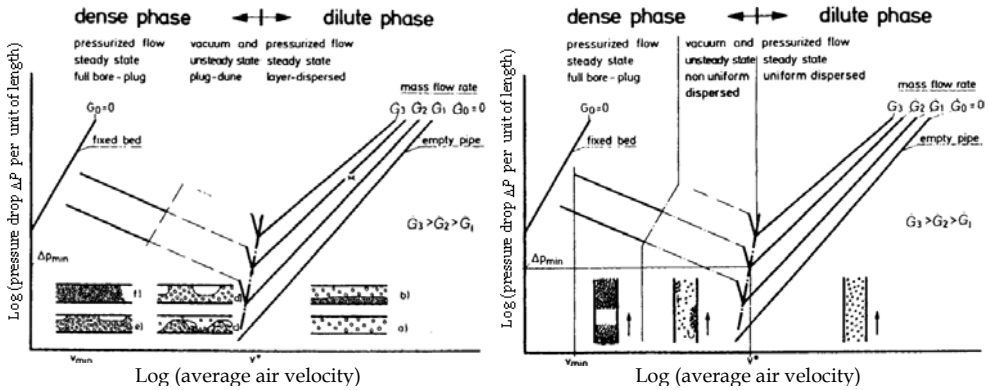

Fig. 7. Conveying conditions showing the changes in solids loading; left: State diagram horizontal flow, right: State diagram vertical flow - source: (Klinzing et al, 1997).

2.1 Pressure drop calculation in the pipeline

The equations given here are based on the hypothesis that the gas-solid flow is in dilute phase. Some assumptions such as: transients in the flow (Basset forces) are not considered nor the pressure gradient around the particles (this is considered negligible in relation to the drag, gravitational and friction forces).

The pressure drop due to particle acceleration is not considered.

The flow is considering incompressible, omnidimensional and the concentration of solids particles is uniform. The physical properties of the two phases are temperature dependent.

The mass flow rate for each phase can be expressed by the following equations:

$$\dot{m}_g = \rho_g V_{mc} \varepsilon_{mc} A \tag{2}$$

$$\dot{G} = \rho_s V_s \varepsilon_s A \tag{3}$$

Where the suffixes g and s denote gas and solid, respectively, V_{mc} is the minimum air velocity in dilute phase in relation to the pipe cross section A, ε_s and ε_{mc} are the volume fraction occupied by the solid and gas inside the pipeline as follows:

$$\varepsilon_s = \frac{A_s}{A} = \frac{4\dot{G}}{\rho_s \pi D^2 V_s} \tag{4}$$

D is the pipe diameter and V_s is the particle velocity. The void or porosity at the minimum air velocity ε_{mc} , in other words is the fraction of volume occupied by the gas (air).

$$\varepsilon_{mc} = \frac{A_g}{A} = 1 - \varepsilon_s \tag{5}$$

Velocity of the particle V_s and the particle terminal velocity V_t calculation:
In this chapter it is considered the models of (Yang, 1978) for the pressure drop calculation.

$$V_s = \frac{V_{mc}}{\varepsilon_{mc}} - V_t \sqrt{1 + \frac{2 f_s V_s^2}{gD} \varepsilon_{mc}^{4.7}} \tag{6}$$

$$V_t = \frac{g d_p^2 \left(\rho_s - \rho_g\right)}{18 \mu_g} \quad , \quad K < 3.3 \tag{7}$$

$$V_t = \frac{0.153 g^{0.71} d_p^{1.14} \left(\rho_s - \rho_g\right)^{0.71}}{\rho_g^{0.29} \mu_g^{0.43}} \quad , \quad 3.3 < K < 43.6 \tag{8}$$

$$V_t = 1.74 \left[\frac{g d_p \left(\rho_s - \rho_g\right)}{\mu_g} \right]^{1/2} \quad , \quad 43.6 < K < 2360 \tag{9}$$

K is a factor that determines the range of validation for the drag coefficient expressions, when the particle Reynolds number is unknown, and given by:

$$K = d_p \left[\frac{g \rho_g \left(\rho_s - \rho_g\right)}{\mu_g^2} \right]^{1/3} \tag{10}$$

Where μ_g is the gas dynamic viscosity, g acceleration due gravity, ρ_g gas (air) density, d_p the particle diameter, f_s is the solid friction factor.
The total pressure drop, ΔP_T for gas-solid flow is calculated with the contribution of the static pressure ΔP_E , and friction loss ΔP_F for both phases:

$$\Delta P_T = \left(\Delta P_E + \Delta P_F\right)_s + \left(\Delta P_E + \Delta P_F\right)_g \tag{11}$$

$$\left(\Delta P_E\right)_s = \rho_s \varepsilon_s L g \tag{12}$$

$$\left(\Delta P_E\right)_g = \rho_g \varepsilon_g L g \tag{13}$$

The contribution due to the friction factor given by the Darcy equation:

$$\left(\Delta P_F\right)_s = \frac{2 f_s \rho_s V_p^2 L}{D} \tag{14}$$

$$\left(\Delta P_F\right)_g = \frac{2 f_g \rho_g V_g^2 L}{D} \tag{15}$$

Where, f_s and f_g are the friction factor for the solid and gas (air), respectively. The friction factor for the gas is calculated by the Colebrook equation.

$$\frac{1}{\sqrt{4f_g}} = 1.74 - 2\log\left[2\xi + \frac{18.7}{\mathrm{Re}\sqrt{4f_g}}\right] \tag{16}$$

$$\mathrm{R}_e = \frac{\rho_g V_{mc} D}{\mu_g} \tag{17}$$

R_e is the Reynolds number, ξ is the relative roughness of the pipe, this equation is implicit for f_g. The friction factors due to solids in vertical and horizontal flow are obtained by the model of (Yang, 1978).

$$f_{sv} = 0.00315\frac{1-\varepsilon_{mc}}{\varepsilon_{mc}^3}\left[\frac{(1-\varepsilon_{mc})V_t}{\frac{V_{mc}}{\varepsilon_{mc}} - V_s}\right]^{-0.979} \tag{18}$$

$$f_{sh} = 0.0293\frac{1-\varepsilon_{mc}}{\varepsilon_{mc}^3}\left[\frac{(1-\varepsilon_{mc})\frac{V_g}{\varepsilon_{mc}}}{\sqrt{gD}}\right]^{-1.15} \tag{19}$$

3. Fundamentals of powder fluidization

Fluidization is an engineering unit operation that occurs when a fluid (liquid or gas) ascend trough a bed of particles, and that particles get a velocity of minimum fluidization V_{mf} enough to suspend the particles, but without carry them in the ascending flow. Since this moment the powder behaves like a liquid at boiling point, that is the reason for term "fluidization". Figure 8 gives a good understanding of the minimum fluidization velocity.

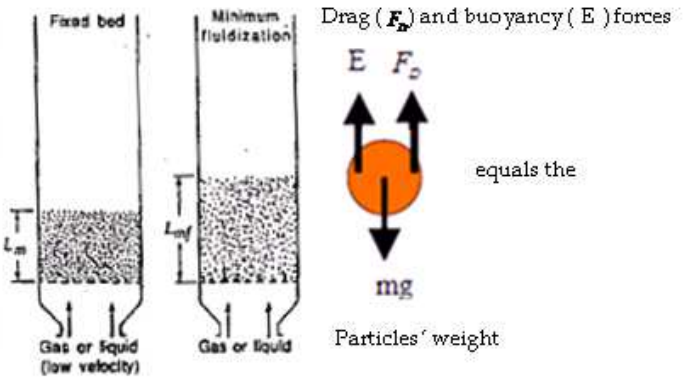

Fig. 8. Fixed and a fluidized bed of particles at a minimum fluidization velocity - adapted from (Kunii & Levenspiel, 1991).

3.1 Minimum fluidization velocity calculation

In this chapter it will be point out the beginning (fluidized beds) and the ending (pneumatic transport) of the flow regime map illustrated in figure 5.

The minimum fluidization velocity will be calculated by the (Ergun, 1952) equation 20 and it's experimental value obtained using a permeameter as showed in figure 19.

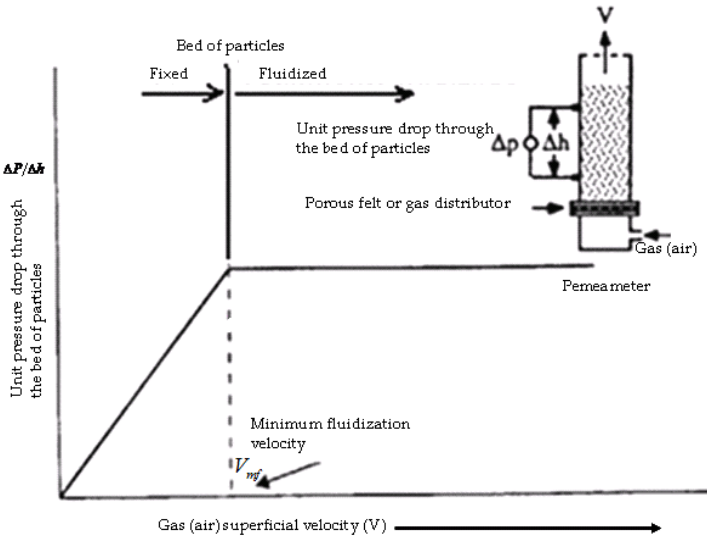

Fig. 9. Pressure drop through a bed of particles versus superficial air velocity – source: (Mills, 1990).

$$(1-\varepsilon_{mf})(\rho_s-\rho_g)g = 150\frac{(1-\varepsilon_{mf})^3}{\varepsilon_{mf}{}^3}\frac{\mu_g V_{mf}}{(\varphi_s d_p)^2} + 1.75\frac{(1-\varepsilon_{mf})}{\varepsilon_{mf}^3}\frac{\rho_g V_{mf}^2}{\varphi_s d_p} = A V_{mf} + B V_{mf}^2 \quad (20)$$

Calculating C by equation 21 we get an equation of second power, which the positive solution is calculated by equation 22.

$$C = (1-\varepsilon_{mf})(\rho_s-\rho_g)g \quad (21)$$

$$V_{mf} = \frac{-A+\sqrt{A^2+4BC}}{2B} \quad (22)$$

Where A and B are the viscous and the inertial factors of the Ergun equation, C is the weight per unit volume of the bed of particles.

Fluidization is related with small velocities, the factor B is negligible and the Ergun equation can be simplified with an error less than 1% by the equation 23.

$$V_{mf} = \frac{C}{A} \Rightarrow V_{mf} = \frac{(\rho_s-\rho_g)g\varepsilon^3{}_{mf}(\phi_s d_p)^2}{150(1-\varepsilon_{mf})\mu_g} \quad (23)$$

For an incipient fluidization, when the weight of particles equals the drag force, it is a good attempt to consider the porosity at the minimum fluidization velocity ε_{mf} equals the porosity ε of the fixed bed. The porosity of the fixed bed is calculated by the equation 24.

$$\varepsilon = 1 - \frac{\rho_{bnv}}{\rho_s} \tag{24}$$

$$\rho_{bnv} = \frac{M_s}{V_{total}} \tag{25}$$

Where ρ_{bnv} is the non-vibrated bulk density, ρ_s is the solid real density calculated in a laboratory by a pycnometer, M_s is the total mass of particles weighted in a electronic scale, V_{total} is the total volume of particles and voids in the sample previously weighted in a electronic scale, d_p is the particle mean diameter obtained by sieve analysis in a laboratory, ϕ_s is the particle sphericity, that can be estimated by equation 26 with d_p in (m).

$$\frac{1-\varepsilon}{\phi_s} = 0.255 Log(d_p) + 1.85 \tag{26}$$

Other important velocity in pneumatic transport and fluidization is the particle terminal velocity V_t that is calculated by equations 7 to 10.

4. Air-fluidized conveyors

4.1 Pile powder flow - simple model

Assuming that the block of alumina is made of non-cohesive material with uniform porosity ε, and is inclined at the moment of analysis in an angle α to the horizontal plane, this elemental block has a constant width Δz.
Also assuming that the flow is isothermal in the (y) direction, a simple force balance requires that:

Gravitational force component = Drag force + Frictional force due to apparent viscosity (27)

$$\rho_s.(1-\varepsilon) g sen\alpha (\Delta x \Delta y \Delta z) = \Delta P(\Delta x \Delta z) + \tau(\Delta y \Delta z) \tag{28}$$

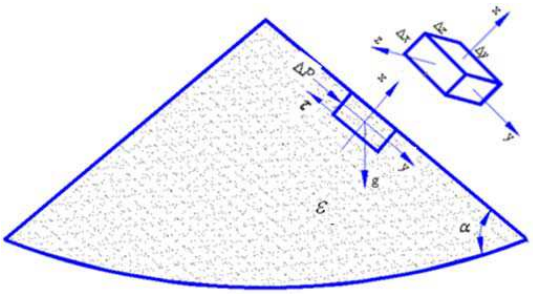

Fig. 10. Force balance acting on an elemental pecked bed block of alumina flowing to repose.

Assuming that the particles of the block are ready to slip over each other, the internal friction between the particles is obtained from equation 29 – source: (Schulze, 2007).

$$\tau_{xy} = \tan\varphi_i . \sigma_x \tag{29}$$

Assuming that the cohesion between particles is negligible, τ_{xy} is the shear stress in the plane parallel to the plane (y-z), ϕ_i is the angle of internal friction of the powder, and σ_x the normal stress in the direction (x) is:

$$\sigma_x = \frac{\rho_s(1-\varepsilon)g\cos\alpha(\Delta x \Delta y \Delta z)}{\Delta y \Delta z} \tag{30}$$

Rearranging the equations 28 to 30 is obtained the pressure drop ΔP of flow in the (y) direction by the equation 31.

$$\frac{\Delta P}{\Delta y} = \rho_s(1-\varepsilon)g(sen\alpha - \tan\varphi_i \cos\alpha) \tag{31}$$

The pile of alumina powder reaches the equilibrium between gravity force and Interparticles forces with an angle of repose β, so in this moment the angle alpha of pile turns beta ($\alpha \rightarrow \beta$).
The friction coefficient between the particles of the pile is the tangent of the particles internal friction angle, given by equation 32.

$$\mu = \tan\phi_i \tag{32}$$

4.2 Engineering model for design proposal to air fluidized conveyors

The proposed model for gas-solid flow is based in the figure 11 and is fitted by the following considerations:

1. The height of the moving fluidized bed in the (y) and (z) directions is constant;
2. The flow of the fluidizing air and that of moving fluidized bed are both steady and full developed in the mean flow;
3. The flow of the moving fluidized bed is in the (y) direction;
4. The slip velocity between the particles and the air in the (y) direction will be negligible;
5. The direction of the fluidizing air will have components in the (x) and (y) directions both in the inlet and outlet of the moving fluidized bed;
6. The pressure of fluidization is constant for every conveyor inclination;
7. The gas-solid flow is considered isothermal and irrotacional;
8. It will not be considered the mass and heat transfer between the particles and the air;
9. The shear stress τ_{xy} of particles will vary in the (x) direction and will be maximum in the bottom and minimum in the top of the elemental block of alumina;
10. The electrostatic and van der Walls forces in the proposed model it will not be considered;
11. The porosity of the moving fluidized bed varies with the fluidizing air velocity but will be considered isotropic;
12. The shear stress of the particles is a function of the moving fluidized bed porosity;

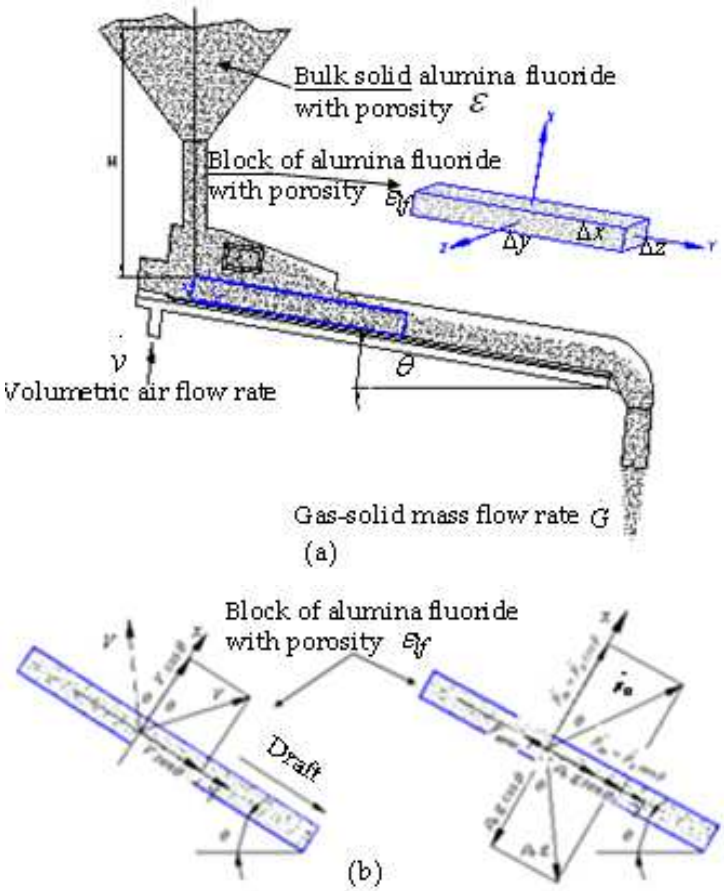

Fig. 11. (a) Elemental block of alumina in an air-fluidized conveyor inclined of an angle θ, (b) in the left: elemental block alumina being fluidized by the components of superficial air velocity V, in the right: balance of forces per unit of volume acting on the elemental block of alumina.

13. The moving fluidized bed has a rheological behavior similar to a liquid;
14. The stress in the side walls of the air fluidized conveyor is considered negligible due to air lubrication,
15. The friction coefficient between particles and the fluidizing felt in the bottom will be minimized by the fluidizing air velocity, and will follow the model of (Kozin & Baskakov, 1996) for angle of repose in the fluidized state, but adjusted with k factor;
16. There will not be rate of mass accumulation inside the air fluidized conveyor see equation 33;
17. It will not have rate of momentum accumulation inside of the air fluidized conveyor see equation 12;
18. The drag force of the particles inside the moving fluidized bed will follow the Ergun (1952) equation.

19. The elemental block of alumina will be considered continuum;
20. The maximum solid mass flow rate will be determined by the model proposed by (Jones, 1965) for powder discharge from small silos – powder liquid-like behavior;
21. For a full opened gate valve of the feed bin the mass flow rate of the assemble bin-air fluidized conveyor will follow the rhythm of the air fluidized conveyor;
22. The model will not consider the contribution of the height of the bulk solids H in the feeding bin.

4.2.1 Equation of continuity

It was assumed in the above considerations that there will not be rate of mass accumulation inside the air fluidized conveyor according to equation 33.

$$\begin{pmatrix}\text{Rate of mass}\\ \text{accumulation}\end{pmatrix}=\begin{pmatrix}\text{Rate of mass}\\ \text{in}\end{pmatrix}-\begin{pmatrix}\text{Rate of mass}\\ \text{out}\end{pmatrix}=0 \tag{33}$$

Equation 33 points out that the mass of gas and solid mixture entering the air fluidized conveyor must be the same as in the outlet of the air fluidized conveyor during the full-developed steady flow regime. So, for the two phases of the flow we have.
Gas phase:

$$\frac{\partial}{\partial x}\varepsilon_{lf}\rho_g V_x+\frac{\partial}{\partial y}\varepsilon_{lf}\rho_g V_y=0 \tag{34}$$

Where: V_x and V_y are the component of the superficial air velocity in the (x) and (y) directions, ρ_g is the gas or air density, ε_{lf} is the moving fluidized bed porosity.
Solid phase:

$$\frac{\partial}{\partial y}(1-\varepsilon_{lf})\rho_s V_s=0 \tag{35}$$

Where: V_s is the velocity of the moving fluidized bed in the (y) direction as it was supposed in the model considerations, ρ_s is the solid or particle density.

4.2.2 The momentum equation

Let's consider the elemental block of alumina in figure 11 with porosity ε_{lf} flowing in a fluid with constant density ρ_g and bulk density ρ_b of the mixture gas-solid and air superficial velocities V_x and V_y in the (x) and (y) directions and the particles flowing in the (y) direction without slipping the air in this direction with velocity V_s.
As it was supposed there will not be rate of momentum accumulation inside of the air fluidized conveyor according to equation 36.

$$0=\begin{pmatrix}\text{Rate of}\\ \text{momentum in}\end{pmatrix}-\begin{pmatrix}\text{Rate of}\\ \text{momentum out}\end{pmatrix}+\begin{pmatrix}\text{Sum of forces}\\ \text{acting on system}\end{pmatrix} \tag{36}$$

The equation 36 is in truth is a force balance equation; the terms used in this equation are as follows:

Rate of momentum in across surface at (x) in the beginning of the elemental block
(Moment transport due to powder apparent viscosity); $\tau_{xy}(\Delta y \Delta z)\big|x$
Rate of momentum in across surface at (x+ Δx) in the end of the elemental block
(Moment transport due to powder apparent viscosity); $\tau_{xy}(\Delta y \Delta z)\big|x + \Delta x$
Rate of momentum in across surface at (y=0)
(Momentum due to gas-solid motion) $(\Delta x \Delta z V_y)(\rho_b V_y)\big|y$
Rate of momentum in across surface at (y + Δy)
(Momentum due to gas-solid motion) $(\Delta x \Delta z V_y)(\rho_b V_y)\big|y + \Delta y$
Pressure force on the elemental block at (x) in the (x) direction $P(\Delta y \Delta z)\big|x$
Pressure force on the elemental block at (x+ Δx) in the(x) direction $P(\Delta y \Delta z)\big|x + \Delta x$
Pressure force on the elemental block at (y=0) in the (y) direction $P(\Delta x \Delta z)\big|y$
Pressure force on the elemental block at ($y_+ \Delta y$) in the (y) direction $P(\Delta x \Delta z)\big|y + \Delta y$
Gravity force acting on the mixture gas-solid in the (x) direction $(\Delta x \Delta y \Delta z)\rho_b g \cos\theta$
Gravity force acting on the mixture gas-solid in the (y) direction $(\Delta x \Delta y \Delta z)\rho_b g sen\theta$
Drag force acting on the mixture gas-solid in the (x) direction F_{Dx}
Drag force acting on the mixture gas-solid in the y) direction F_{Dy}
Friction force due to gravity and fluid during block motion in the(y) direction $F_{friction}$
Substituting the terms relating with (x) direction in the moment balance equation 36 results:

$$P(\Delta y \Delta z)\big|x - P(\Delta y \Delta z)\big|x + \Delta x - F_{Dx} + (\Delta x \Delta y \Delta z)\rho_b g \cos\theta = 0 \tag{37}$$

Equation 11 is now divided by the elemental volume $\Delta x \Delta y \Delta z$ and, if Δx is allowed to be infinitely small $\Delta x \to 0$, it is obtained:

$$\frac{\partial P}{\partial x} = \rho_b g \cos\theta - \bar{F}_{Dx} \tag{38}$$

Where $\bar{F}_{Dx}$ is the drag force per unit of volume of the elemental block in (x) direction.
Substituting the terms relating with (y) direction in the moment balance equation 10 results equation 39:

$$\tau_{xy}(\Delta y \Delta z)\big|x - \tau_{xy}(\Delta y \Delta z)\big|x + \Delta x + (\Delta x \Delta z V_y)(\rho_b V_y)\big|y - (\Delta x \Delta z V_y)(\rho_b V_y)\big|y + \Delta y +$$

$$+ P(\Delta x \Delta z)\big|y - P(\Delta x \Delta z)\big|y + \Delta y + (\Delta x \Delta y \Delta z)\rho_b g sen\theta + F_{Dy} - F_{friction} = 0 \tag{39}$$

Equation 37 is now divided by the elemental volume $\Delta x \Delta y \Delta z$ and, if Δx and Δy are allowed to be infinitely small $\Delta x \to 0$ and $\Delta y \to 0$ it is obtained:

$$-\frac{\partial \tau_{xy}}{\partial x} - \rho_b V_y \frac{\partial V_y}{\partial y} - \frac{\partial P}{\partial y} + \bar{F}_{Dy} - \bar{F}_{friction} + \rho_b g sen\theta = 0 \tag{40}$$

One of the considerations of the proposed model is that the particle velocity doesn't vary in the (y) direction, so the second term of equation 40 is zero. Rearranging the equation 40, it is obtained:

$$\frac{\partial P}{\partial y} = \bar{F}_{Dy} - \frac{\partial \tau_{xy}}{\partial x} - \bar{F}_{friction} + \rho_b g sen\theta \tag{41}$$

Where $\bar{F}_{Dy}$, the drag force per unit of volume of the elemental block in the (y) direction is calculated concerning the 18th consideration of the proposed model as follows:
$\bar{F}_{Dy}$ is calculated by the Ergun equation 42

$$\bar{F}_{Dy} = 150\frac{(1-\varepsilon_{lf})^2}{\varepsilon_{lf}^3}\frac{\mu_g V_y}{(\varphi_s d_p)^2} + 1{,}75\frac{(1-\varepsilon_{lf})}{\varepsilon_{lf}^3}\frac{\rho_g V_y^2}{\varepsilon_{lf}^3(\varphi_s d_p)}, \varepsilon_{lf} < 0{,}79 \tag{42}$$

$\bar{F}_{friction}$ is the force due to gravity and drag forces of the moving fluidized bed in the (y) direction.

$$\bar{F}_{friction} = \mu_a \frac{\partial P}{\partial x} \tag{43}$$

Substituting the equation 38 in equation 43 we get.

$$\bar{F}_{friction} = \mu_a(\rho_b g\cos\theta - \bar{F}_{Dx}) \tag{44}$$

$$\bar{F}_{Dx} = AV_x + BV_x^2 \tag{45}$$

$$\mu_a = \tan\left[(1-0.1\frac{V}{V_{mf}})^2\phi_i\right] \tag{46}$$

$$\bar{F}_{Dy} = AV_y + BV_y^2 \tag{47}$$

$$A = 150\frac{(1-\varepsilon_{lf})^2}{\varepsilon_{lf}{}^3}\frac{\mu_g}{(\varphi_s.d_p)^2} \tag{48}$$

$$B = 1.75\frac{(1-\varepsilon)}{\varepsilon_{lf}{}^3}\frac{\rho_g}{\varphi_s d_p} \tag{49}$$

$$V_x = V\cos\theta \tag{50}$$

$$V_y = Vsen\theta \tag{51}$$

$$\bar{F}_{Dx} = AV\cos\theta + BV^2\cos^2\theta \tag{52}$$

$$\bar{F}_{Dy} = AVsen\theta + BV^2 sen^2\theta \tag{53}$$

A and B are the viscous and inertial factors of Ergun's equation, these factors are calculated by the equations 48 and 49, μ_a is the coefficient of friction between the particles and the bottom of the air fluidized conveyor at fluidized state.

If we reanalyze the equation 28 it is possible to compare the fluidized powder flowing rather like a liquid, which is sheared by the powder apparent viscosity and the friction due to inertia force. Therefore, by rearranging equation 28, we can obtain the maximum shear stress in the bottom of the block of height h and length of Δy by equation 54.

$$-\tau_{0xy} = -\rho_b g sen\theta h + \mu_a \rho_b g \cos\theta \frac{h^2}{L} \tag{54}$$

In the plane parallel with the bottom arising shear stress as a function of the deepness of the block in the (x) direction calculated by equation 55.

$$\tau_{xy} = -\rho_b g \cos\theta \left[(2\mu_a \frac{h}{L} - \tan\theta)(h-x) - \mu_a \frac{(h-x)^2}{L} \right] - \tau_{0xy} \tag{55}$$

Equation 55 describes the shear stress distribution and is according to the considerations of the proposed model. In others words, in the top of the block (x equals 0) the shear stress is minimum and maximum in the bottom of the block (x equals h).
Deriving equation 55, it is found the shear stress gradient by equation 56.

$$-\frac{\partial \tau_{xy}}{\partial x} = -\rho_b g \left[2\frac{\mu_a}{L} x \cos\theta - sen\theta \right] \tag{56}$$

Algebraically rearranging the equations 43 to 53 and introducing the results in equation 41, we get:

$$\frac{\partial P}{\partial y} = AVK_1 + BV^2K_2 + \rho_b g K_3 \tag{57}$$

$$K_1 = sen\theta + \mu_a \cos\theta \tag{58}$$

$$K_2 = sen^2\theta(1-\mu_a) + \mu_a \tag{59}$$

$$k_3 = 2sen\theta - \mu_a \cos\theta (2\frac{x}{L} + 1) \tag{60}$$

Equation 34 represents a weight of bulk solids per unit of volume of the elemental block of alumina as can be seen in figure 11. The elemental block of alumina flows in the (y) direction with porosity less than 0.8 in an air-fluidized conveyor inclined at an angle θ in relation to the horizontal plane, with (x equals h – height of the bed) and a length of L meters long.
Rearranging 57 as weight of bulk solids by its total volume we get equation 61.

$$\frac{\Delta mg}{\Delta V_{total}} = AVK_1 + BV^2K_2 + \rho_b g K_3 \tag{61}$$

Dividing the left side of equation 61 by the time (t) and integrating it, we get the mass solid flow rate of the air-fluidized conveyor in equation 62.

$$\dot{G} = \frac{AVK_1 + BV^2K_2 + \rho_b gK_3}{g}\dot{v} \tag{62}$$

Where Δm and ΔV_{total} are the mass and total volume of the elemental block of alumina, $\dot{m}$ is the mass solid flow rate predicted to the air-fluidized conveyor, $\dot{v}$ is the volumetric flow rate of the fluidizing air, V is the superficial air velocity, V_{mf} is the minimum fluidization velocity.

$$V = \frac{\dot{v}}{\Delta z \Delta y} \tag{63}$$

$$V_s = \frac{\dot{G}}{\rho_b A} \tag{64}$$

Where $\Delta z = b$, $\Delta y = L$ and A are the width, length and cross section of the air fluidized conveyor.
According to (Jones, 1965), the flow of bulk solids from a small silo (bin) or from an orifice in the bottom of a fluidized bed, behaves like a liquid flowing and is calculated by the energy balance equation of Bernoulli as follows in the equation 65 adjusted by a reduction of 50% of the liquid flow from in the same condition.

$$\dot{G} = 0,5\rho_b A_o \sqrt{2gH} \tag{65}$$

$$\rho_b = (1-\varepsilon)\rho_s \tag{66}$$

Where $\dot{m}$ is the solid mass flow rate, ρ_b is the solid bulk density, A_o is the area of the bin's discharge orifice (normally the orifice has a gate valve to control the mass solid flow rate) ε is the material packed or non-aerated porosity, g is the acceleration due to gravity and H is the height of bulk solid material in the bin - see figure 11.

5. Pipeline feeding devices

There are many feeding device used in pneumatic conveying of solids. Low pressure devices are used in dilute phase conveyor such as venture feeder and rotary airlock valve as is illustrated in figure 12a. For pneumatic conveying in dense phase blow vessel is used a as is illustrated in figure 12b.
The feeding device must guarantee a good sealing between the pipeline and the bag house, hopper or silo used to collect or store the powder that will be pneumatically conveyed.

6. Petro coke handling at Albras anode bake furnace

Albras increased its productive capacity of 350,000 t/y to 390,000 t/y in the year 2000. To reach this production it was necessary to increase the bake furnaces capacity and, in consequence to increase the furnaces suction system capacity, which at that time didn't comply with efficiency the current demand of the plant.

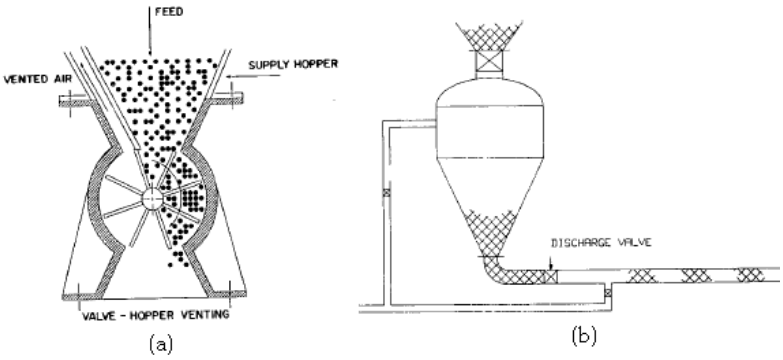

Fig. 12. Feeding devices used in pneumatic conveying of powders – source: (Klinzing *et al*, 1997).

The Carbon Plant Engineering Group accepts the challenge to upgrade the original system to increase the coke suction capacity of 15 t/h to 80 t/h. So software in FORTRAN was developed using the equations 1 to 19 to calculate the pressure drop in the circuit showed in figure 13, and to specify a new exhauster, redesign the bag house, the telescope tube and a new nozzle.
Following, the steps of the project, from the coke characterization and the circuit topology.

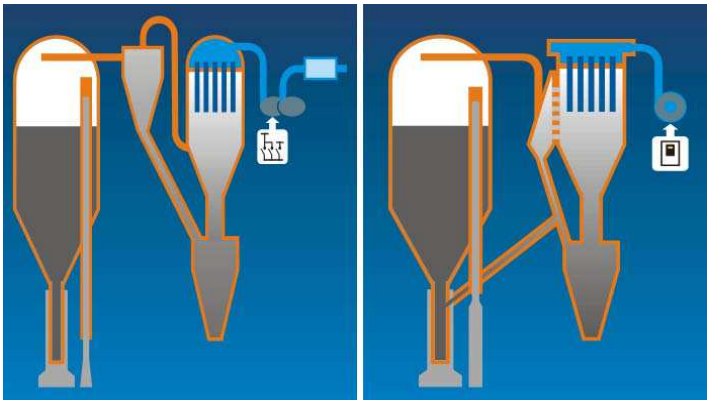

Fig. 13. Bake furnace suction system – old system in the left, new system in the right – source: (Vasconcelos, 2000).

The system capacity was increased from 15 t/h to 110 t/h of coke suction capacity. Figure 14 shows the nozzle details of the old and new systems.

7. Petro coke handling at Albras carbon plant

In smelters that use prebaked anodes, operations such as butt cleaning, butt and anode reject crushing and grinding, handling of coke packing material in the bake furnace, floor sweeping and discharge of dust from bake furnace cranes cause significant problems with the high generation of carbon dust and consequent environmental pollution.

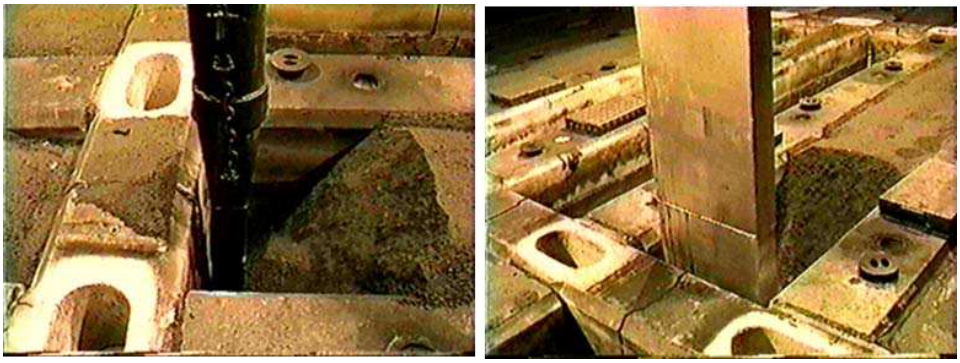

Fig. 14. Albras bake furnace coke suction system before and after modifications – source: Albras Alumínio Brasileiro SA.

To control the dust pollution is a very difficult task. Another problem is how to convey and store the dust collected.
This case study presents the problem existing in the carbon plant of Albras, describing the pneumatic conveyor system developed by the Carbon Plant Engineering department, and the storage of the dust collected in the carbon plant.
Using the same software developed by the team of professor Mesquita of Federal Univerty of Pará to collect the carbon dust from the bake furnace and rodding shop and pneumatic convey to a silo in the paste plant at Albras aluminum smelter.
Figure 15 presents the originals problems relating the emission of carbon dust during the carbon plant process.

Fig. 15. Petro coke handling problem at Albras, in left bake furnace, in center and in the right bag house dust discharge at the rodding shop - source: Albras Alumínio Brasileiro SA.

Figure 16 shows the situation of coke handling at the bake furnaces during the multipurpose overhead crane coke dust discharge. The ultra fine carbon dust is generated during the pack and unpacked coke used to cover the anodes to avoid air-oxidation and facilitate the heat transfer to anode during the baking process.
Figure 17 shows the computer screen of a pneumatic conveying in dilute phase developed to collect the carbon dust in the carbon plant reducing the pollution in the workplace. The dust

collect is send to a cement plant reducing the consumption of charcoal in the cement's process.

Fig. 16. Dust discharging at Albras bake furnace, implemented solution in the left side, in the center discharge of dust in big bags, free falling of dust in truck in the right - source: Albras Alumínio Brasileiro SA.

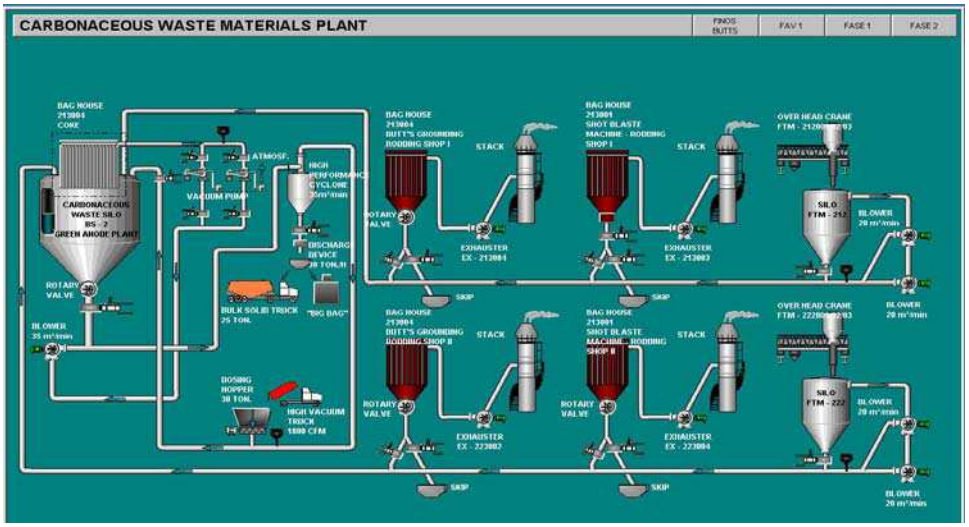

Fig. 17. Computer screen of a pneumatic conveying system in dilute phase at Albras aluminum smelter – source: (Vasconcelos & Mesquita, 2003).

8. Air fluidized conveyor

It was developed a non-conventional air slide called air fluidized conveyor to be of low weight, non-electrical conductor, heat resistant, easy to install, maintain and also operates at a very low cost compared with the conventional air slides. Figure 18 shows in the left a conventional air slide with rectangular shape, with one inlet and one outlet and in the right the round air fluidized conveyor with possibility to have multiples outlets.

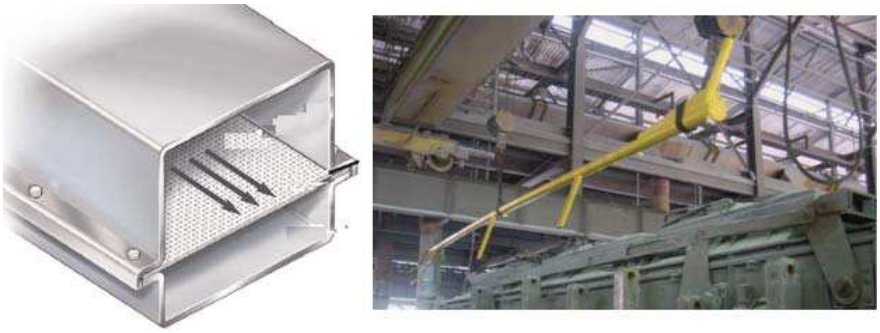

Fig. 18. The Albras aluminum smelter air fluidized conveyor and a conventional air slide in the left.

8.1 Predict and experimental results of the air fluidized conveyor for fluoride alumina

The properties calculated and obtained from experiments with alumina fluoride used at Albras aluminum smelter are summarized in table 2.

Material property	value
Specific gravity	3.5
Non- aerated/vibrated bulk density - kg/m^3	1000
Aerated bulk density at ($0.5\,V_{mf}$) - kg/m^3	999.66
Aerated bulk density at ($0.75\,V_{mf}$) - kg/m^3	999.66
Aerated bulk density at ($0.875\,V_{mf}$) - kg/m^3	999.66
Aerated bulk density at ($1.0\,V_{mf}$) - kg/m^3	990.86
Aerated bulk density at ($1.5\,V_{mf}$) - kg/m^3	868.47
Aerated bulk density at ($2.0\,V_{mf}$) - kg/m^3	786.86
Aerated bulk density at ($2.5\,V_{mf}$) - kg/m^3	726.77
Minimum fluidization velocity by Ergun equation (cm/s)	1.83
Minimum fluidization velocity - experimental (cm/s)	1.77
Mean particle diameter - μm	99.44
Non- aerated angle of repose - °	35
Non- aerated angle of internal friction - °	70
Normal packed porosity (-)	0.71428
Geldart classification according figure 4 – group	B

Table 2. Properties of the alumina fluoride.

Figure 19 shows the pictures of the permeameters used to determine experimentally the minimum fluidization velocity of alumina fluoride.

Fig. 19. Permeameters used at Albras laboratory to survey the minimum fluidization velocity of the powders used in the primary aluminum industry - source: Albras Alumínio Brasileiro SA.

8.2 Predict and experimental results of the air fluidized conveyor for alumina fluoride

Two air-fluidized conveyors using the equation 62 were developed as result of a thesis for doctorate. The results for the conveyor with diameter of 3 inches and 1.5 m long showed in figure 20 are summarized in table 3.

Fig. 20. Air-fluidized conveyor of 1.5 m long with three outlets.

Mass gas-solid flow rate for alumina fluoride (t/h) - air fluidized conveyor of (3"/1.5m)							Inclination (°)
0	0	0	0	1.973	4.400	6.965	(-1)
0	0	0	0	2.145	4.616	7.222	(-0.5)
0	0	0	0.109	2.317	4.831	7.478	0
0	0	0	0.359	2.660	5.261	7.990	1
0	0	0	0.608	3.002	5.689	8.499	2
0	0	0	0.858	3.344	6.116	9.005	3
40	60	70	80	120	160	200	Air flow rate (LPM)
0.5	0.75	0.875	1	1.5	2	2.5	V/V_{mf}

Table 3. Predicted solid mass flow rate of a 3″-1.5 m air-fluidized conveyor based on equation 62.

The experimental results for the air-fluidized conveyor showed in figure 20 are summarized in table 4.

Mass gas-solid flow rate for alumina fluoride (t/h) - air fluidized conveyor of (3"/1.5m)							Inclination (°)
0	0	0	2.148	4.709	6.173	7.978	(-1)
0	0	0	2.825	5.871	7.633	8.649	(-0.5)
0	0	0.944	3.563	6.448	8.099	8.851	0
0	1.293	3.529	4.952	7.787	8.917	9.127	1
0	2.778	4.261	6.002	8.478	10.523	10.309	2
0	3.192	4.829	6.208	9.764	11.497	13.195	3
40	60	70	80	120	160	200	Air flow rate (LPM)
0.5	0.75	0.875	1	1.5	2	2.5	V/V_{mf}

Table 4. Experimental results from the tests runs at Albras Aluminum smelter laboratory.

Figure 21 shows the other air-fluidized conveyor of 3 inches diameter and 9.3 m long designed using equation 62, which will be used as prototype to feed continuously the electrolyte furnace with alumina fluoride.

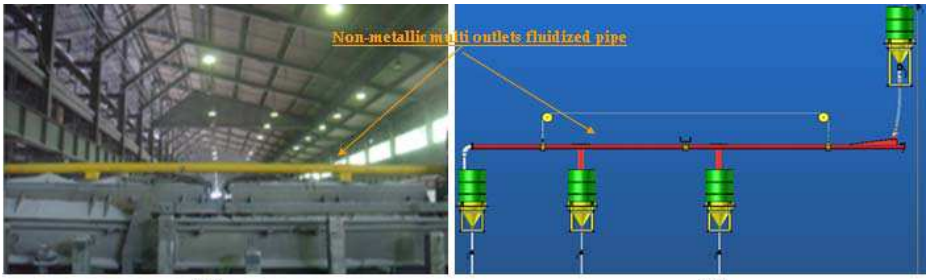

Fig. 21. a) The nonmetallic fluidized pipe during tests in electrolytic aluminum cell; b) Sketch of the nonmetallic fluidized pipe for performance test at the fluidization laboratory.

The equation 62 predicts a mass solid flow rate of 7.29 t/h for that conveyor, but observed was a mass solid flow rate of 6.6 t/h at $1.5\,V_{mf}$ and a downward inclination of 0.5° was used during the test run depicted in figure 22.

Fig. 22. Test rig to measure the mass solid flow rate of a, 9.3 m long 3 inches diameter air-fluidized conveyor at Albras aluminum smelter.

9. Conclusion

The objective of this chapter is to contribute with readers responsible for the design and operation of industrial furnaces.
Focused on the project of powder handling at high velocity, such as the two cases studies concerning pneumatic conveying in dilute phase applied at Albras aluminum smelter. The last case study regarding powder handling at very low velocity such is illustrated in figure 5 is used in several industrial applications and the intention in this case is to help project engineers to design air slides of low energy consumption. Based on the desired solid mass flow rate of the process using equation 62 is possible to design the conveyor, knowing the rheology of the powder that will be conveyed. In the application of Albras aluminum smelter the experiments results for the small conveyor the values obtained in the experiments was higher than that predict for horizontal and upward inclination in velocities less than the minimum fluidization velocity, because the equation doesn't take in to account the height of material in the feeding bin according (Jones, 1965) equation. In the case of the larger conveyor we have better results, because the conveyor is fed by a fluidized hose as can be seen in figure 21b. So in the next steps of the research it will be necessary to include the column H of the feeding bin in equation 62.

10. Acknowledgment

The authors would like to thanks the LORD GOD for this opportunity, Albras Alumínio Brasileiro SA for the authorization to public this chapter, the Federal University of Pará for my doctorate in fluidization engineering and to inTech - Open Access Publisher for the virtuous circle created to share knowledge between readers and authors.

11. References

Ergun, S. Fluid Flow through Packed Columns, Chem. Engrg. Progress, Vol. 48, No. 2, pp. 89 – 94 (1952).

Geldart, D. Types of Gas Fluidization Powder Technology, 7, 285 – 292 (1972 – 1973).

Jones, D. R. M. Liquid analogies for Fluidized Beds, Ph.D. Thesis, Cambridge, 1965.

Klinzing, G. E.; Marcus, R. D.; Risk, F. & Leung, L. S. Pneumatic Conveying of Solids – A Theoretical and Practical Approach, second edition, Chapman Hall. (1997).

Kozin, V. E.; Baskakov, A. & Vuzov, P., Izv., Neft 1 Gas 91 (2) (1996).

Kunii, D. & Levenspiel O. Fluidization Engineering, second edition, Butterworth-Heinemann, Boston (1991).

Mills, D. Pneumatic Conveying Design Guide, Butterworths, London, (1990).

Schulze, D. Powder and Bulk Solids, Behavior, Characterization, Storages and Flow, Spriger Heidelberg, New York (2007).

Vasconcelos, P.D. Improvements in the Albras Bake Furnaces Packing and Unpacking System – Light Metals 2000, pp. 493 – 497.

Vasconcelos, P.D & Mesquita, A. L. Exhaustion Pneumatic Conveyor and Storage of Carbonaceous Waste Materials - Light Metals 2003, pp. 583-588.

Yang, W. C. A mathematical definition of choking phenomenon and a mathematical model for predicting choking velocity and choking voidage, AIChE J., Vol. 21, 1013 (1978).

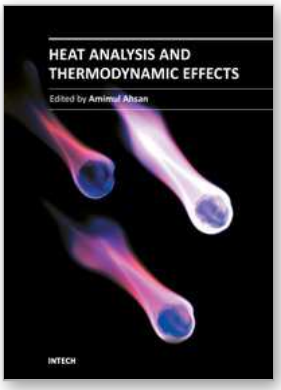

Heat Analysis and Thermodynamic Effects

Edited by Dr. Amimul Ahsan

ISBN 978-953-307-585-3
Hard cover, 394 pages
Publisher InTech
Published online 22, September, 2011
Published in print edition September, 2011

The heat transfer and analysis on heat pipe and exchanger, and thermal stress are significant issues in a design of wide range of industrial processes and devices. This book includes 17 advanced and revised contributions, and it covers mainly (1) thermodynamic effects and thermal stress, (2) heat pipe and exchanger, (3) gas flow and oxidation, and (4) heat analysis. The first section introduces spontaneous heat flow, thermodynamic effect of groundwater, stress on vertical cylindrical vessel, transient temperature fields, principles of thermoelectric conversion, and transformer performances. The second section covers thermosyphon heat pipe, shell and tube heat exchangers, heat transfer in bundles of transversely-finned tubes, fired heaters for petroleum refineries, and heat exchangers of irreversible power cycles. The third section includes gas flow over a cylinder, gas-solid flow applications, oxidation exposure, effects of buoyancy, and application of energy and thermal performance index on energy efficiency. The forth section presents integral transform and green function methods, micro capillary pumped loop, influence of polyisobutylene additions, synthesis of novel materials, and materials for electromagnetic launchers. The advanced ideas and information described here will be fruitful for the readers to find a sustainable solution in an industrialized society.

How to reference

In order to correctly reference this scholarly work, feel free to copy and paste the following:

Paulo Douglas Santos de Vasconcelos and André Luiz Amarante Mesquita (2011). Gas-Solid Flow Applications for Powder Handling in Industrial Furnaces Operations, Heat Analysis and Thermodynamic Effects, Dr. Amimul Ahsan (Ed.), ISBN: 978-953-307-585-3, InTech, Available from: http://www.intechopen.com/books/heat-analysis-and-thermodynamic-effects/gas-solid-flow-applications-for-powder-handling-in-industrial-furnaces-operations

INTECH
open science | open minds

InTech Europe
University Campus STeP Ri
Slavka Krautzeka 83/A
51000 Rijeka, Croatia
Phone: +385 (51) 770 447
Fax: +385 (51) 686 166

InTech China
Unit 405, Office Block, Hotel Equatorial Shanghai
No.65, Yan An Road (West), Shanghai, 200040, China
中国上海市延安西路65号上海国际贵都大饭店办公楼405单元
Phone: +86-21-62489820
Fax: +86-21-62489821